


Quantitatively Monitoring *In Situ* Mitochondrial Thermal Dynamics by Upconversion Nanoparticles

Xiangjun Di, Dejiang Wang, Jiajia Zhou, Lin Zhang, Martina H. Stenzel, Qian Peter Su,* and Dayong Jin*

 Cite This: *Nano Lett.* 2021, 21, 1651–1658

 Read Online

ACCESS |

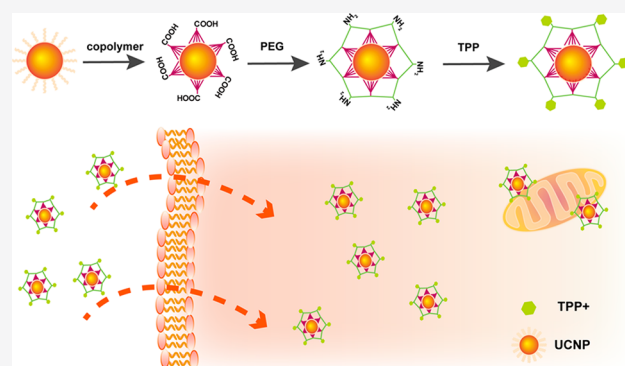
 Metrics & More

 Article Recommendations

 Supporting Information

ABSTRACT: Temperature dynamics reflect the physiological conditions of cells and organisms. Mitochondria regulate the temperature dynamics in living cells as they oxidize the respiratory substrates and synthesize ATP, with heat being released as a byproduct of active metabolism. Here, we report an upconversion nanoparticle-based thermometer that allows the *in situ* thermal dynamics monitoring of mitochondria in living cells. We demonstrate that the upconversion nanothermometers can efficiently target mitochondria, and the temperature-responsive feature is independent of probe concentration and medium conditions. The relative sensing sensitivity of $3.2\% \text{ K}^{-1}$ in HeLa cells allows us to measure the mitochondrial temperature difference through the stimulations of high glucose, lipid, Ca^{2+} shock, and the inhibitor of oxidative phosphorylation. Moreover, cells display distinct response time and thermodynamic profiles under different stimulations, which highlight the potential applications of this thermometer to study *in situ* vital processes related to mitochondrial metabolism pathways and interactions between organelles.

KEYWORDS: Upconversion Nanoparticles (UCNPs), Biosensing, Nanothermometry, Mitochondria



INTRODUCTION

Intracellular temperature is a crucial parameter to assess the status of living cells and organisms.¹ The activations of a wide range of chemical reactions in the living cell, especially in the mitochondria, produces a large amount of energy and causes a change in temperature. As the powerhouse of the cell, mitochondria provide energy to the living cell through the oxidative phosphorylation process.² During this chemical reaction, about 67% of the energy is used to synthesize ATP, and the other ~33% dissipates in the form of heat.³ Failure to produce ATP will cause a change in mitochondria temperature; therefore, the variation of the mitochondria temperature indicates the cellular metabolism status.⁴ Given its importance to fundamental studies, disease diagnosis, and therapy, accurate and specific temperature sensing at a subcellular scale remains as a challenge due to the lack of noninvasive sensing probes.^{5–8}

Fluorescence nanothermometry has emerged to non-invasively reveal the localized intracellular temperature in living cells.⁹ Temperature-responsive fluorescent materials,^{10–12} including small molecules,¹³ fluorescent polymers,¹ fluorescent proteins,¹⁴ and inorganic particles,^{15,16} have been extensively explored. For example, Homma et al. developed a ratiometric nanothermosensor (Mito-RTP) using thermosensitive rhodamine B and thermo-insensitive CS NIR dye, which enables the temperature monitoring of mitochondria under

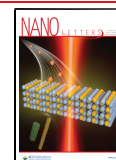
chemical stimulation.¹³ Yang et al. designed photoluminescence spectral-shifts quantum dots (QDots) to monitor the temperature change in NIH/3T3 cells under Ca^{2+} stress and cold shock.¹⁵ However, due to the concern of photobleaching as well as photoblinking issues, these fluorescent nanothermometers are limited in the area of long-term tracking and sensing.

Lanthanide-doped upconversion nanoparticles (UCNPs) with unique nanophotonic characteristics are suitable for long-term biosensing, bioimaging,^{17,18} and photothermal therapy¹⁹ as UCNPs are optically stable²⁰ and biologically compatible.²¹ The anti-Stokes emission process, upon NIR light excitation, avoids cellular autofluorescence and can minimize the potential photodamage to cells as well as allowing deep tissue penetration.²¹ UCNP nanothermometers were first demonstrated to monitor the temperature change of living cells upon external heating.²² UCNPs doped with

Received: October 30, 2020

Revised: January 19, 2021

Published: February 6, 2021



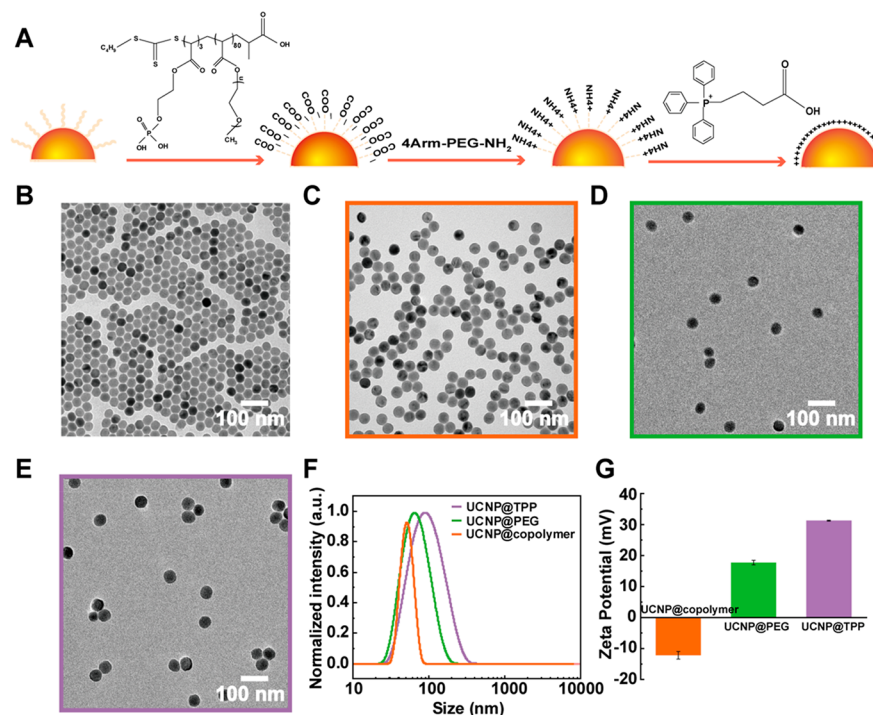


Figure 1. Characterization of UCNP thermosensors. (A) Schematic illustration of the mitochondria-targeted probes with cross-linked polymer layers and TPP. (B–E) Representative TEM images of UCNPs, UCNPs@copolymer, UCNPs@PEG, and UCNPs@TPP, respectively. (F) DLS for UCNPs with different surface modifications. (G) ζ -Potential of UCNPs with different surface modifications.

erbium ions display a temperature-dependent luminescence following the Boltzmann distribution²²

$$\frac{I_{525}}{I_{545}} = C \exp\left(-\frac{\Delta E}{kT}\right)$$

where I_{525} and I_{545} are the integrated fluorescent intensities around the 525 and 545 nm emission peaks, respectively, C is a constant, ΔE is the energy gap, k is the Boltzmann constant, and T is the absolute temperature. Recently, UCNP nanothermometers were further applied for *in vivo* temperature monitoring in small-animal imaging.^{17,23} Several other remarkable works also include the Nd³⁺-doped UCNPs to sense temperature changes in NIH/3T3 cells¹⁷ and a hybrid structure composed of PbS quantum dots and Tm-doped UCNPs to realize intratumoral monitoring *in vivo*.²³ Although clear advances have been made, there remains a large gap to enable UCNP thermometry with an *in situ* organelle targeting capability for localized intracellular temperature sensing. The key is to functionalize UCNPs to become biocompatible and specific to the target organelle, otherwise the relatively large UCNPs (e.g., 20 nm) with positive charges from the trivalent lanthanide ions exposed on the surface tend to be aggregated, less stable in physiological environment, and cause the issue of nonspecific bindings.²⁴

In this study, by using mitochondria-targeting, temperature-dependent, and nonphotobleaching UCNPs, we monitor the *in situ* mitochondrial temperature dynamics under different nutrient conditions and chemical stimulations. A cross-linked polymer network was applied to avoid the aggregation of UCNPs in the cell culture medium.²⁵ PEGMEMA₈₀-*b*-EGMP₃ diblock copolymers were further modified with 4Arm-PEG-NH₂ to allow the mitochondria-targeting moiety (3-carboxypropyl)triphenylphosphonium bromide (TPP) to be covalently functionalized onto UCNPs. This strategy leads to

UCNPs capable of targeting mitochondria,^{26,27} as the large membrane-potential gradient from the cell plasma to mitochondria allows the stepwise accumulation of TPP⁺ from initially in-cell plasma to mitochondria.²⁷ The practicality of the intracellular temperature-sensing strategy was validated by the real-time monitoring of the mitochondrial temperature variations induced by external nutrient conditions and chemical stimulations, including glucose, lipid, Ca²⁺, and the inhibitor of oxidative phosphorylation. With the nanothermometer, mitochondria display reaction-time and thermal dynamics profiles under different physiological nutrient conditions and chemical stimulations. Interestingly, mitochondria respond faster and remain at a relatively high-temperature level long in high oleic acid versus a high-glucose culture medium, which indicates different pathways of glycometabolism and lipid metabolism. The difference in distinct thermodynamics highlights the extensive applications of a mitochondria-targeting nanothermometer to study vital biological processes related to mitochondrial metabolism pathways and interactions between mitochondria and other organelles, such as lysosome, ER,²⁸ Golgi,²⁹ lipid droplet, and peroxisome.³⁰

■ DESIGN OF UCNPs@TPP

The method to synthesize UCNPs was described previously (see more details in the [Materials and Methods](#) section of the [Supporting Information](#)).³¹ To construct a stable and mitochondria-targeting nanothermometer, a cross-linked polymer network was applied to functionalize UCNPs on the surface (Figure 1A).²⁵ These hydrophilic cross-linked coating layers can firmly anchor onto the surface of positively charged UCNPs and keep UCNPs stable in both the cell culture medium and the intracellular environment. The transmission electron microscopy (TEM) images (Figure 1B–E) show the

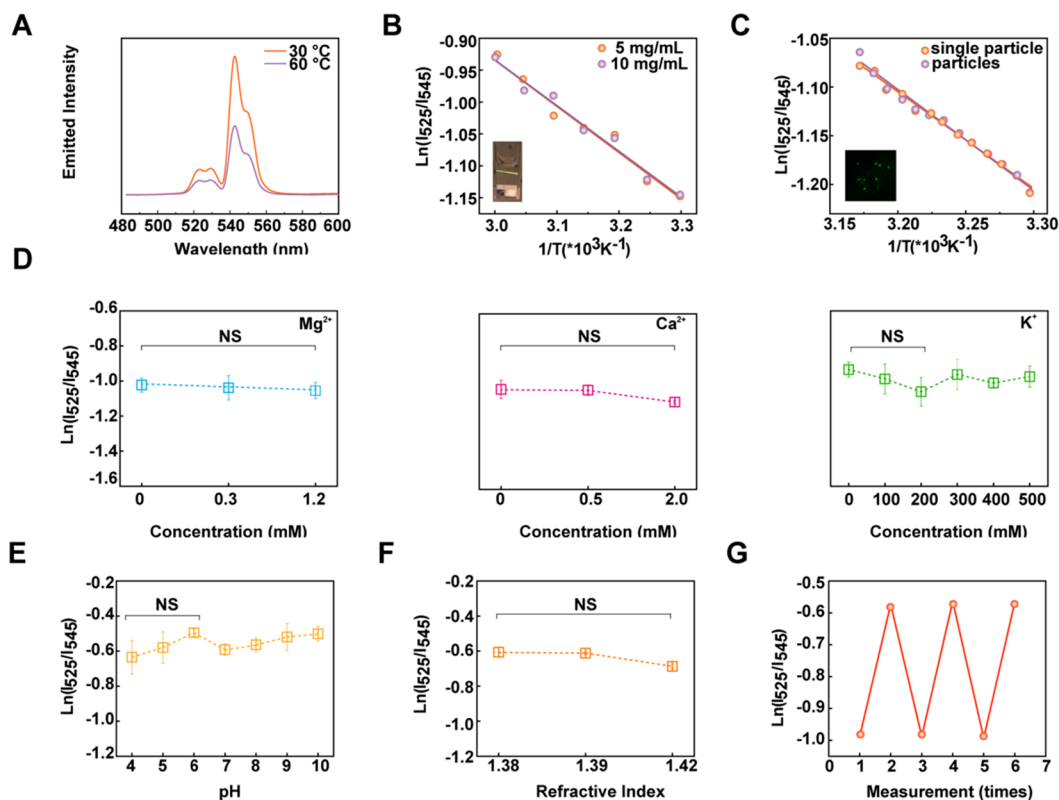


Figure 2. Thermoresponsive properties of UCNPs@TPP in vitro. (A) Upconversion emission spectra obtained at two different cuvette temperatures ($\lambda_{\text{exc}} = 980$ nm). (B) Plots of $\ln(I_{525}/I_{545})$ vs $1/T$ to calibrate the thermometric scale in the solution with different concentrations. (C) Plots of $\ln(I_{525}/I_{545})$ vs $1/T$ to calibrate the thermometric scale at the single-particle level versus the multiple-particle level. (D) Thermal sensitivity of UCNPs@TPP in response to Mg^{2+} (left), Ca^{2+} (middle), or K^{+} (right) ($n = 3$ independent experiments). (E) Changes in the $\ln(I_{525}/I_{545})$ ratio of UCNPs@TPP in response to the pH ($n = 3$ independent experiments). (F) Changes in the $\ln(I_{525}/I_{545})$ ratio of UCNPs@TPP in response to the refractive index ($n = 3$ independent experiments). (G) Reversibility of the temperature-dependent changes of the UCNPs@TPP fluorescence. The solution temperature changed from 30 to 45 °C. Data points represent the mean \pm SD

morphology uniformity and monodispersity of the UCNPs before and after the surface functionalization. The size of UCNPs increased from 31.09 ± 2.76 nm for the as-synthesized UCNPs to 39.43 ± 1.64 , 42.34 ± 2.54 , and 45.13 ± 2.55 nm (measured by TEM in Figure 1B–E, respectively). The dynamic light scattering (DLS) results (Figure 1F) confirmed the high uniformity with the peak values, with the hydrodynamic size increasing from 51.77 to 72.08 and 103.10 nm after each step of the surface modifications. For TPP conjugation, the amine groups of 4Arm-PEG-NH₂ on the cross-linked polymer network provide the anchoring groups for TPP. The ζ -potential results (Figure 1G) indicated the successful modification of each step, as the surface charge changed from -13 to 18 mV with the exposure of 4Arm-PEG-NH₂ and to a further positive value of 32 mV with TPP by a carbodiimide reaction.^{32,33} The strong positive charge on the UCNPs' surface facilitate the nanoparticles to travel into cell cytoplasm and mitochondria.²⁷ Using ATR-FTIR, the characteristic absorption of P=O stretches at 1102 cm^{-1} confirmed the PEGMEMA₈₀-b-EGMP₃ diblock copolymer grafted on the surface of UCNPs compared with the spectra of UCNPs@oleic acid (UCNPs@OA) as shown in Figure S1A, and the appearance of =C–H stretching vibration bands from an aromatic ring located in the ranges of 3100 – 3000 cm^{-1} and 752 – 636 cm^{-1} confirmed the presence of TPP on the UCNPs' surface. Furthermore, the long-term stability of UCNPs@TPP was tested by DLS (Figure S1B). These UCNPs@TPP bioconjugates exhibited excellent stabilities in

both the incubation medium (Dulbecco's Modified Eagle's Medium (DMEM) containing 2% v/v fetal bovine serum (FBS) and 0.5% v/v BSA) and the complete medium (DMEM containing 10% FBS and 1% v/v penicillin–streptomycin), as shown in Figure S1C.

■ THERMoresponsive PROPERTIES OF UCNPs@TPP IN VITRO

Under the 980 nm excitation, UCNPs@TPP emitted a green emission consist of two distinct bands between 515–535 nm (centered at 525 nm) and 535–570 nm (centered at 545 nm) (Figure 2A), which were attributed to the $^2\text{H}_{11/2}$ and $^4\text{S}_{3/2}$ transitions of Er^{3+} , respectively. While the emitted intensities at both the 525 and 545 nm peaks decreased when the temperature increased from 30 to 60 °C due to thermal quenching, the ratio of the 525 and 545 nm peaks increased following Boltzmann distribution (Figure 2B).

An accurate calibration curve is extremely crucial to quantitatively analyze temperature dynamics in the intracellular environment.⁹ Ideal fluorescent thermosensors should be independent of the concentration, as it is difficult to control and measure the concentration of fluorescent thermosensors in living cells. As shown in Figure 2B, the residual sum of squares (RSS) of these two linear fittings was measured as 0.013159 by calibrating two solutions containing different concentrations of UCNPs@TPP (5 and 10 mg/mL) using a purpose-built spectrometer, indicating that UCNPs@TPP as a fluorescent

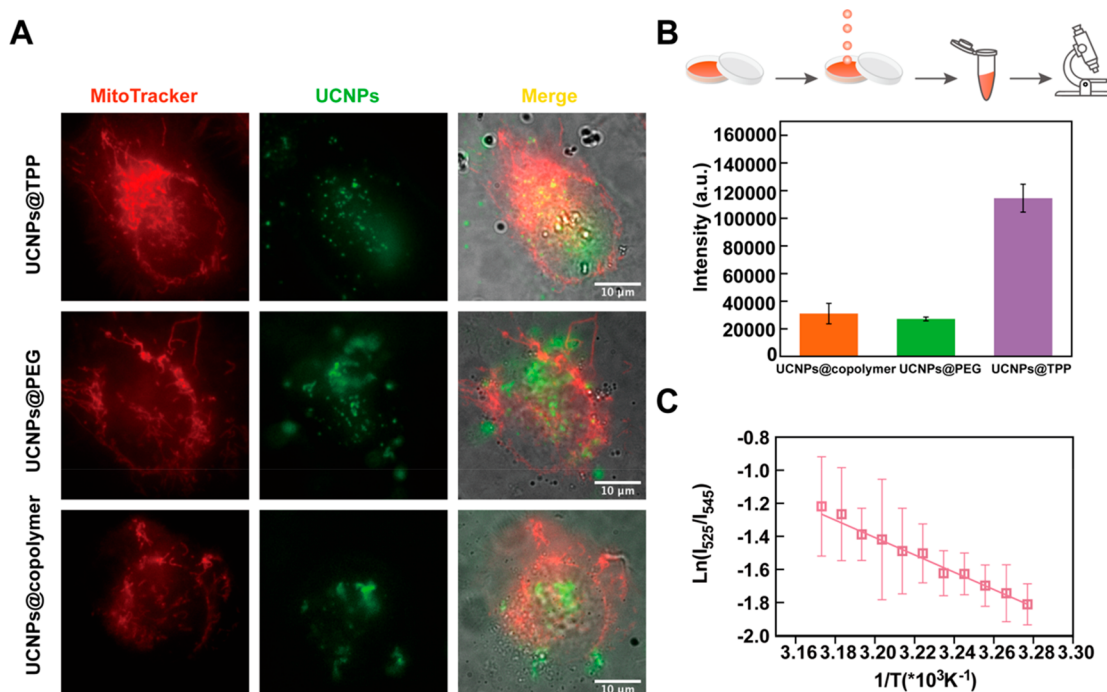


Figure 3. Temperature-dependent fluorescence characteristics of UCNP@TPP targeted to *in situ* mitochondria in HeLa cells. (A) Intracellular colocalization of UCNP@TPP with MitoTracker (the red channel is MitoTracker Deep Red excited by a 647 nm laser, the green channel is UCNP@TPP excited by a 980 nm laser, and the gray channel is the bright-field images). (B) The fluorescence intensity of isolated mitochondria treated with UCNP@TPP ($n = 10$ fields of view from three independent repeats). (C) Plot of $\ln(I_{525}/I_{545})$ vs $1/T$ to calibrate the thermometric scale in HeLa cells ($n = 10$ cells). Data points represent the mean \pm SD, and the scale bar is 10 μm .

thermosensor is concentration-independent. To confirm this result, the calibration curves at the single-particle level were performed with a purpose-built total internal-reflected fluorescent (TIRF) microscopy system. Although the calibration results obtained by microscope were distinct from those obtained by the spectrometer due to the different sensitivities of the spectrometer with a photomultiplier tube (PMT) detector and the microscope with an electron-multiplying CCD (EMCCD) camera, the RSS of these two linear fittings was measured as 0.00482. Notably, the thermal responsiveness of UCNP@TPP was essentially unchanged under different concentrations no matter whether from the single-particle level or in the solution.

The microenvironment conditions in living cells, such as ionic strength, pH value, and refractive index, vary as time and locations change as well as from one organelle to another.⁹ For example, the refractive indexes of the cell cytoplasm, nucleus, and mitochondria are 1.38, 1.39, and 1.42 respectively.³⁴ The performance of fluorescent thermosensors should remain stable in the living cell. Figure 2D–F illustrates that temperature-dependent fluorescence of UCNP@TPP was not affected by Mg^{2+} or Ca^{2+} at different physiological intracellular concentrations, ionic strengths (0–500 mM), pH levels (4–10), and refractive indexes (1.38–1.42). Furthermore, the I_{525}/I_{545} ratios of UCNP@TPP can be reproduced by heating and cooling between 30 and 45 °C for multiple cycles, demonstrating the reversibility of UCNP@TPP without thermal denaturation. Since the absorption spectrum of water is in the range of 680–1000 nm with a peak at 980 nm, we monitored the temperature variations of UCNP@TPP excited by a 980 nm laser at an intensity of 0.5 kW/cm^2 for 30 min. As shown in Figure S2, the illumination of

a 0.5 kW/cm^2 980 nm laser did not lead to a temperature increase of the water within 30 min.

■ UCNP@TPP WORKS AS A SUBCELLULAR THERMOSENSOR IN HELA CELLS

To apply UCNP@TPP in live cells, we first checked the cytotoxicity of UCNP@TPP in live cells with short-time treatments at different concentrations measured by MTT test experiments. Figure S3A shows that the cell viability in the experimental groups was similar to that of the control group, indicating that UCNP@TPP has a negligible cytotoxicity to HeLa cells. Considering the labeling efficiency, 50 $\mu\text{g}/\text{mL}$ was chosen in the following live-cell experiments.

Next, the exact locations of nanoparticles in the live cell were tested. Colocalizations of UCNP@TPP and MitoTracker Deep Red were conducted by a purpose-built TIRF microscope with 980 and 647 nm lasers as the light sources. As shown in Figure 3A, the green channel illustrates that these three kinds of nanoparticles dispersed into HeLa cells after 12 h of incubation. UCNP@copolymer and UCNP@PEG preferred to form aggregates, while UCNP@TPP dispersed well within the cell. The merged images show that UCNP@TPP had a better colocalization than the control groups. Pearson's R -value for the experimental group was 0.70. In contrast, Pearson's R -values for the UCNP@PEG and UCNP@copolymer treatment groups were 0.40 and 0.27, respectively. These results indicated that UCNP@TPP preferred to target mitochondria. Since the temporal and spatial resolutions in microscopy imaging may affect the accuracy of the colocalization results, we further confirmed the locations of UCNP@TPP by isolating mitochondria from HeLa cells using a mitochondria isolation kit (Thermo Fisher) dispersed in 50 μL of PBS buffer. The mitochondria

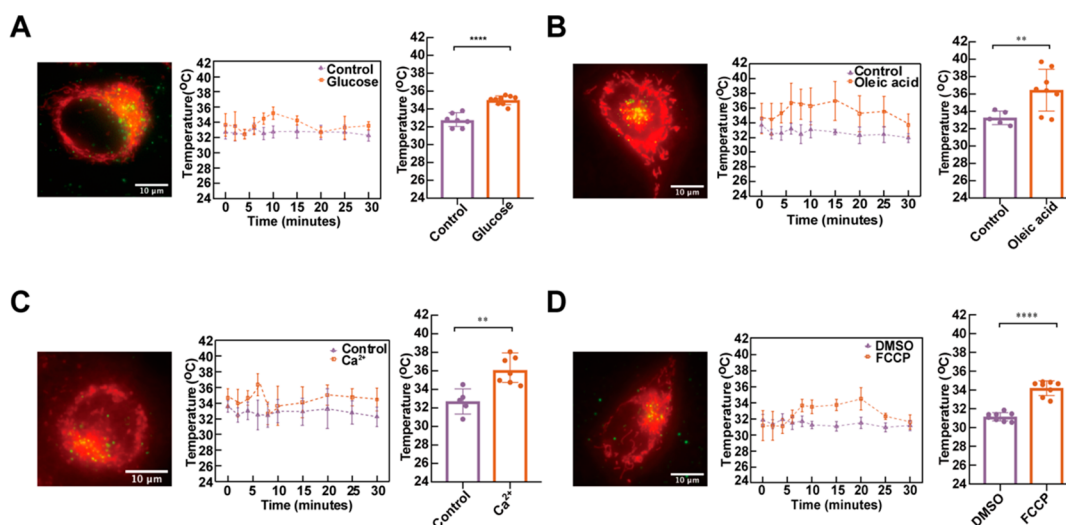


Figure 4. Visualization of mitochondrial thermal dynamics in HeLa cells response to nutrient and chemical stimulations. (A) UCNP@TPP images (left) and mitochondrial temperature dynamics (middle) in the presence of 5 mg/mL glucose within 30 min, and Student's *t* test of both no glucose and glucose at 10 min ($p < 0.0001$, right). (B) UCNP@TPP images (left) and mitochondrial temperature variations (middle) in the presence of 5 μ M oleic acid within 30 min, and Student's *t* test of both no oleic acid and oleic acid at 15 min ($p < 0.05$, right). (C) UCNP@TPP images (left) and mitochondrial temperature changes (middle) in the presence of 1 μ M ionomycin calcium salt within 30 min, and Student's *t* test of both no calcium and calcium at 6 min ($p < 0.05$, right). (D) UCNP@TPP images (left) and mitochondrial temperature fluctuations (middle) in the presence of 10 μ M FCCP within 30 min, and Student's *t* test of both DMSO and FCCP at 10 min ($p < 0.0001$, right). The temperatures in panels A–D were calculated by the calibration plot in Figure 3C; $n = 5$ –8 cells for panels A–D, and data points represent the mean \pm SD. The merged-cell images in A–D are MitoTracker (red) and UCNPs@TPP (green) from different treatments.

suspension was transferred to a 96-well plate and dried at room temperature, and the fluorescence intensity of the isolated mitochondria was measured (Figures 3B and S3B). In the control groups (Figure 3B) with UCNPs@PEG and UCNPs@copolymer, the fluorescence intensities of the nanoparticles were barely seen, while the intensity of UCNPs@TPP treated group was $\sim 3\times$ higher than those of the other two control groups, indicating the successful mitochondria targeting.

Furthermore, to rule out the possible interactions between UCNPs@TPP and lysosomes, HeLa cells were stained with LysoTracker. After 4 h of incubation, HeLa cells were washed with PBS. UCNPs@TPP dispersed into the HeLa cells with faster than the control groups, and there were more nanoparticles delivered to the cells, suggesting the facilitating role of the mitochondrial-targeting moiety TPP. The merged images showed that UCNPs@TPP already escaped from lysosomes as a result of the good lipophilicity of TPP (Figure S4).

The above results allowed us to plot the calibration curves in HeLa cells. By changing the extracellular temperature of the cell culture using a temperature-controllable incubator on top of the microscope system, the logarithmic value of the I_{525}/I_{545} ratio showed a much more gradual and linear fluorescence change in the range of 32–42 $^{\circ}\text{C}$ relative to the reciprocal temperature (Figure 3C), suggesting that UCNPs@TPP is a quantitative nanothermosensor in living cells. The equation of the calibration curve was $y = -5.33x + 15.657$ ($R^2 = 0.98144$, Pearson's $R = -0.99068$). The relative sensing sensitivity in HeLa cells at 32 $^{\circ}\text{C}$ was 3.2% K^{-1} , and the temperature resolution was ~ 2.3 K.

■ VISUALIZATION OF MITOCHONDRIAL THERMAL DYNAMICS IN HELA CELLS

We then applied UCNPs@TPP to monitor the mitochondrial temperature variations induced by external nutrient conditions

and chemical stimulations. First, we tested a high glucose medium in regard to HeLa cells. Glucose produces pyruvate in the cytosol and then participates in the Krebs Cycle in mitochondria, which generates heat. In the HeLa cells incubated with UCNPs@TPP, the mitochondria temperature increased significantly by 2.25 $^{\circ}\text{C}$ in the first 10 min with the addition of 5 mg/mL glucose ($P < 0.0001$ by Students' *t*-test) (Figure 4A, right), before recovering to the original level after 20 min of treatment. As for the control group with the addition of the same amount of PBS, the mitochondrial temperature remained stable within 30 min (Figure 4A).

Oleic acid was then tested as an alternative nutrient source. Columns in Figure 4B demonstrate that the mitochondrial temperature increased by 2.74 $^{\circ}\text{C}$ only 5 min after adding 5 μ M oleic acid in the culture medium, but the mitochondrial temperature did not recover to the original level even after 30 min of treatment. Compared with glucose treatment, the oleic acid treatment takes the mitochondrial temperature to a higher peak value with a faster speed and a longer plateau time, indicating the different metabolism pathways and energy efficiencies for glucose and oleic acid.

The mitochondrial temperature in living cells can be elevated by Ca^{2+} shock, as it can promote the pumping of ions and accelerate respiration reactions.³⁵ Ionomycin calcium salt is an ionophore that makes the cell membrane highly permeable for Ca^{2+} .³⁶ Here, Figure 4C showed that the temperature of the mitochondria increased sharply within 6 min after adding 1 μ M ionomycin calcium salt before dropping back within another 2 min (Figure 4C). Ionomycin calcium salt induces intracellular stress, possibly causing damage to mitochondria in HeLa cells.³⁵ Furthermore, carbonyl cyanide-4-(trifluoromethoxy)phenylhydrazone (FCCP) was tested as a chemical stimulator in HeLa cells. FCCP is an inhibitor of oxidative phosphorylation, which disrupts ATP synthesis by transporting protons across the mitochondrial inner mem-

brane.³⁷ During this process, mitochondria release a large amount of heat. In the HeLa cells incubated with UCNPs@TPP, the mitochondrial temperature increased by almost 2 °C in the first 10 min after adding 10 μM FCCP ($P < 0.0001$ by Students' *t* test) (Figure 4D). In the following 20 min, the mitochondrial temperature kept increasing by ~1 °C. Mitochondria eventually recovered to the original temperature after 30 min of FCCP treatment. In comparison, the temperature in the control group remained at a similar level after the DMSO treatment. These results provide evidence that UCNPs@TPP works as a precise subcellular thermosensor for monitoring the mitochondrial thermodynamics.

CONCLUSION AND DISCUSSION

Intracellular temperature, especially mitochondrial thermodynamics, is one of the most crucial biophysical parameters to assess the status of living cells and organisms, which is related to homeostasis and energy balance.³⁸ Toward the development of a precise nanothermosensor for use both *in vitro* and in living cells, we have synthesized a series of UCNPs@copolymer, UCNPs@PEG, and UCNPs@TPP nanosensors. We applied the nonphotobleaching ratiometric nanothermosensor to monitor the *in situ* mitochondrial thermodynamics under different physiological and chemical stimuli. The UCNPs@TPP conjugate enables us to monitor the glucose-, lipid-, Ca²⁺-, and FCCP-dependent thermodynamics in the mitochondria within living HeLa cells. UCNPs@TPP is a powerful tool for analyzing how the mitochondria metabolism activates and maintains cellular homeostasis in living cells. The distinct thermodynamics highlight the extensive applications of nanothermometers to study vital biological processes related to mitochondrial metabolism and interactions between mitochondria and other organelles, such as lysosome, ER,²⁸ Golgi,²⁹ lipid droplet, and peroxisome.³⁰

Chretien et al. recently reported that the mitochondrial temperature reached >323 K (50 °C) using MitoThermo Yellow (MTY) in HEK293T cells treated with an oxygen-rich buffer to fully functionalize the respiration.³⁹ An intracellular temperature measurement using organic dyes is not suitable for long-term monitoring purposes. Hu et al. reported another large increase in the temperature using plasmonic nanostructures with Au nanoparticles in the cytoplasm of CaSki cells during active Ca²⁺ transportation.⁴⁰ Intracellular temperature measurement using inorganic probes requires a precise calibration in the extracellular environment and the accurate colocalization of organelles with a specific targeting organelle. A fluorescent protein (FP)-based thermometer was also reported in HeLa cells by Nakano et al. with a 6–9 °C temperature increase, which is consistent with our results.⁴¹ A comparison of different thermometers will be meaningful, including fluorescent proteins,⁴¹ organic dyes,^{13,39} plasmonic materials,⁴⁰ UCNPs-based²³ nanothermometer for living cells, etc.

The unique optical properties of UCNPs allow us to track long-term thermodynamics in mitochondria across cell cycles or even in live deep tissues with the NIR excitation wavelength in the future.^{10,11,42} The bioconjugation system we developed will allow us to establish a library of different organelle-targeted nanothermometers, such as lysosome, ER, and Golgi. Combined with other mitochondria evaluation methods, including live-cell super-resolution imaging,^{43,44} an *in vitro* reconstitution assay,^{2,45} and near-infrared deep tissue imaging,¹⁹ the UCNPs-based mitochondrial nanothermometer will

be a powerful platform for multifunctional imaging, sensing,⁴⁶ therapy,¹⁹ and even tracking the pace of life.⁴⁷

ASSOCIATED CONTENT

Supporting Information

The Supporting Information is available free of charge at <https://pubs.acs.org/doi/10.1021/acs.nanolett.0c04281>.

Materials and experimental procedures, ATR-FTIR spectra, biostability of nanoparticles, phototoxicity of the laser, MTT experiments, colocalization of nanoparticles with LysoTracker, and the data analysis process (PDF)

AUTHOR INFORMATION

Corresponding Authors

Qian Peter Su – Institute for Biomedical Materials & Devices (IBMD), Faculty of Science and School of Biomedical Engineering, Faculty of Engineering and Information Technology, University of Technology Sydney, Sydney, NSW 2007, Australia; orcid.org/0000-0001-7364-3945; Email: qian.su@uts.edu.au

Dayong Jin – Institute for Biomedical Materials & Devices (IBMD), Faculty of Science, University of Technology Sydney, Sydney, NSW 2007, Australia; UTS-SUSTech Joint Research Centre for Biomedical Materials & Devices, Department of Biomedical Engineering, Southern University of Science and Technology, Shenzhen, China 518055; Email: dayong.jin@uts.edu.au

Authors

Xiangjun Di – Institute for Biomedical Materials & Devices (IBMD), Faculty of Science, University of Technology Sydney, Sydney, NSW 2007, Australia

Dejiang Wang – Institute for Biomedical Materials & Devices (IBMD), Faculty of Science, University of Technology Sydney, Sydney, NSW 2007, Australia

Jiajia Zhou – Institute for Biomedical Materials & Devices (IBMD), Faculty of Science, University of Technology Sydney, Sydney, NSW 2007, Australia; orcid.org/0000-0002-0605-5745

Lin Zhang – Cluster for Advanced Macromolecular Design, School of Chemistry, University of New South Wales, Sydney, NSW 2052, Australia

Martina H. Stenzel – Cluster for Advanced Macromolecular Design, School of Chemistry, University of New South Wales, Sydney, NSW 2052, Australia; orcid.org/0000-0002-6433-4419

Complete contact information is available at: <https://pubs.acs.org/doi/10.1021/acs.nanolett.0c04281>

Author Contributions

X.D., Q.P.S., J.Z., M.S., and D.J. designed the project; X.D. prepared UCNPs and conjugates; X.D., D.W., L.Z., and Q.P.S. built the optical system, performed experiments, and analyzed data; X.D., Q.P.S., and D.J. wrote the paper; and Q.P.S. and D.J. supervised the studies.

Notes

The authors declare no competing financial interest. The data that support the findings of this study are available from the corresponding author upon reasonable request.

ACKNOWLEDGMENTS

The authors acknowledge the financial support from the Australia National Health and Medical Council (NHMRC, APP1177374 to Q.P.S.), the Australia National Heart Foundation (NHF, 102592 to Q.P.S.), the Australian Research Council Discovery Early Career Researcher Award Scheme (DE180100669 to J. Z.), the National Natural Science Foundation of China (NSFC, 61729501), the Major International (Regional) Joint Research Project of NSFC (51720105015), the Science and Technology Innovation Commission of Shenzhen (KQTD20170810110913065), the Australia China Science and Research Fund Joint Research Centre for Point-of-Care Testing (ACSRF658277, SQ2017YFGH001190), and the China Scholarship Council (no. 201706170028 to X.D. and no. 201706170027 to D.W.).

REFERENCES

(1) Inada, N.; Fukuda, N.; Hayashi, T.; Uchiyama, S. Temperature imaging using a cationic linear fluorescent polymeric thermometer and fluorescence lifetime imaging microscopy. *Nat. Protoc.* **2019**, *14* (4), 1293–1321.

(2) Wang, C.; Du, W.; Su, Q. P.; Zhu, M.; Feng, P.; Li, Y.; Zhou, Y.; Mi, N.; Zhu, Y.; Jiang, D.; Zhang, S.; Zhang, Z.; Sun, Y.; Yu, L. Dynamic tubulation of mitochondria drives mitochondrial network formation. *Cell Res.* **2015**, *25* (10), 1108–20.

(3) Huang, Z.; Li, N.; Zhang, X.; Wang, C.; Xiao, Y. Fixable Molecular Thermometer for Real-Time Visualization and Quantification of Mitochondrial Temperature. *Anal. Chem.* **2018**, *90* (23), 13953–13959.

(4) Rango, M.; Arighi, A.; Bonifati, C.; Del Bo, R.; Comi, G.; Bresolin, N. The brain is hypothermic in patients with mitochondrial diseases. *J. Cereb. Blood Flow Metab.* **2014**, *34* (5), 915–20.

(5) del Rosal, B.; Ximenes, E.; Rocha, U.; Jaque, D. In Vivo Luminescence Nanothermometry: from Materials to Applications. *Adv. Opt. Mater.* **2017**, *5* (1), 1600508.

(6) Jaque, D.; Vetrone, F. Luminescence nanothermometry. *Nanoscale* **2012**, *4* (15), 4301–26.

(7) Ruiz, D.; del Rosal, B.; Acebrón, M.; Palencia, C.; Sun, C.; Cabanillas-González, J.; López-Haro, M.; Hungría, A. B.; Jaque, D.; Juárez, B. H. Ag/Ag₂S Nanocrystals for High Sensitivity Near-Infrared Luminescence Nanothermometry. *Adv. Funct. Mater.* **2017**, *27* (6), 1604629.

(8) Suzuki, M.; Tseeb, V.; Oyama, K.; Ishiwata, S. Microscopic detection of thermogenesis in a single HeLa cell. *Biophys. J.* **2007**, *92* (6), L46–8.

(9) Zhou, J.; del Rosal, B.; Jaque, D.; Uchiyama, S.; Jin, D. Advances and challenges for fluorescence nanothermometry. *Nat. Methods* **2020**, *17* (10), 967–980.

(10) Green, K.; Huang, K.; Pan, H.; Han, G.; Lim, S. F. Optical Temperature Sensing With Infrared Excited Upconversion Nanoparticles. *Front. Chem.* **2018**, *6*, 416.

(11) Zhou, J.; Chizhik, A. I.; Chu, S.; Jin, D. Single-particle spectroscopy for functional nanomaterials. *Nature* **2020**, *579* (7797), 41–50.

(12) Brites, C. D. S.; Lima, P. P.; Silva, N. J. O.; Millán, A.; Amaral, V. S.; Palacio, F.; Carlos, L. D. Thermometry at the nanoscale. *Nanoscale* **2012**, *4* (16), 4799–4829.

(13) Homma, M.; Takei, Y.; Murata, A.; Inoue, T.; Takeoka, S. A ratiometric fluorescent molecular probe for visualization of mitochondrial temperature in living cells. *Chem. Commun. (Cambridge, U. K.)* **2015**, *51* (28), 6194–7.

(14) Donner, J. S.; Thompson, S. A.; Kreuzer, M. P.; Baffou, G.; Quidant, R. Mapping Intracellular Temperature Using Green Fluorescent Protein. *Nano Lett.* **2012**, *12* (4), 2107–2111.

(15) Yang, J. M.; Yang, H.; Lin, L. Quantum dot nano thermometers reveal heterogeneous local thermogenesis in living cells. *ACS Nano* **2011**, *5* (6), 5067–71.

(16) Okabe, K.; Sakaguchi, R.; Shi, B.; Kiyonaka, S. Intracellular thermometry with fluorescent sensors for thermal biology. *Pfluegers Arch.* **2018**, *470* (5), 717–731.

(17) Shi, Z.; Duan, Y.; Zhu, X.; Wang, Q.; Li, D.; Hu, K.; Feng, W.; Li, F.; Xu, C. Dual functional NaYF₄:Yb(3+), Er(3+)/NaYF₄:Yb(3+), Nd(3+) core-shell nanoparticles for cell temperature sensing and imaging. *Nanotechnology* **2018**, *29* (9), 094001.

(18) Wen, S.; Zhou, J.; Zheng, K.; Bednarkiewicz, A.; Liu, X.; Jin, D. Advances in highly doped upconversion nanoparticles. *Nat. Commun.* **2018**, *9* (1), 2415.

(19) Zhu, X.; Feng, W.; Chang, J.; Tan, Y. W.; Li, J.; Chen, M.; Sun, Y.; Li, F. Temperature-feedback upconversion nanocomposite for accurate photothermal therapy at facile temperature. *Nat. Commun.* **2016**, *7*, 10437.

(20) Wu, S.; Han, G.; Milliron, D. J.; Aloni, S.; Altoe, V.; Talapin, D. V.; Cohen, B. E.; Schuck, P. J. Non-blinking and photostable upconverted luminescence from single lanthanide-doped nanocrystals. *Proc. Natl. Acad. Sci. U. S. A.* **2009**, *106* (27), 10917–21.

(21) Nam, S. H.; Bae, Y. M.; Park, Y. I.; Kim, J. H.; Kim, H. M.; Choi, J. S.; Lee, K. T.; Hyeon, T.; Suh, Y. D. Long-term real-time tracking of lanthanide ion doped upconverting nanoparticles in living cells. *Angew. Chem., Int. Ed.* **2011**, *50* (27), 6093–7.

(22) Vetrone, F.; Naccache, R.; Zamarron, A.; Juarranz de la Fuente, A.; Sanz-Rodriguez, F.; Martinez Maestro, L.; Martin Rodriguez, E.; Jaque, D.; Garcia Sole, J.; Capobianco, J. A. Temperature sensing using fluorescent nanothermometers. *ACS Nano* **2010**, *4* (6), 3254–8.

(23) Qiu, X.; Zhou, Q.; Zhu, X.; Wu, Z.; Feng, W.; Li, F. Ratiometric upconversion nanothermometry with dual emission at the same wavelength decoded via a time-resolved technique. *Nat. Commun.* **2020**, *11* (1), 4.

(24) Muhr, V.; Wilhelm, S.; Hirsch, T.; Wolfbeis, O. S. Upconversion Nanoparticles: From Hydrophobic to Hydrophilic Surfaces. *Acc. Chem. Res.* **2014**, *47* (12), 3481–3493.

(25) Zhong, Y.; Ma, Z.; Wang, F.; Wang, X.; Yang, Y.; Liu, Y.; Zhao, X.; Li, J.; Du, H.; Zhang, M.; Cui, Q.; Zhu, S.; Sun, Q.; Wan, H.; Tian, Y.; Liu, Q.; Wang, W.; Garcia, K. C.; Dai, H. In vivo molecular imaging for immunotherapy using ultra-bright near-infrared-IIb rare-earth nanoparticles. *Nat. Biotechnol.* **2019**, *37* (11), 1322–1331.

(26) Wang, X. H.; Peng, H. S.; Yang, L.; You, F. T.; Teng, F.; Hou, L. L.; Wolfbeis, O. S. Targetable phosphorescent oxygen nanosensors for the assessment of tumor mitochondrial dysfunction by monitoring the respiratory activity. *Angew. Chem., Int. Ed.* **2014**, *53* (46), 12471–12475.

(27) Zielonka, J.; Joseph, J.; Sikora, A.; Hardy, M.; Ouari, O.; Vasquez-Vivar, J.; Cheng, G.; Lopez, M.; Kalyanaraman, B. Mitochondria-Targeted Triphenylphosphonium-Based Compounds: Syntheses, Mechanisms of Action, and Therapeutic and Diagnostic Applications. *Chem. Rev.* **2017**, *117* (15), 10043–10120.

(28) Qin, J.; Guo, Y.; Xue, B.; Shi, P.; Chen, Y.; Su, Q. P.; Hao, H.; Zhao, S.; Wu, C.; Yu, L.; Li, D.; Sun, Y. ER-mitochondria contacts promote mtDNA nucleoids active transportation via mitochondrial dynamic tubulation. *Nat. Commun.* **2020**, *11* (1), 4471.

(29) Hao, H.; Niu, J.; Xue, B.; Su, Q. P.; Liu, M.; Yang, J.; Qin, J.; Zhao, S.; Wu, C.; Sun, Y. Golgi-associated microtubules are fast cargo tracks and required for persistent cell migration. *EMBO Rep.* **2020**, *21* (3), No. e48385.

(30) Valm, A. M.; Cohen, S.; Legant, W. R.; Melunis, J.; Hershberg, U.; Wait, E.; Cohen, A. R.; Davidson, M. W.; Betzig, E.; Lippincott-Schwartz, J. Applying systems-level spectral imaging and analysis to reveal the organelle interactome. *Nature* **2017**, *546* (7656), 162–167.

(31) Wang, M.; Abbineni, G.; Cleverger, A.; Mao, C.; Xu, S. Upconversion nanoparticles: synthesis, surface modification and biological applications. *Nanomedicine* **2011**, *7* (6), 710–29.

(32) Wang, X. H.; Peng, H. S.; Yang, L.; You, F. T.; Teng, F.; Tang, A. W.; Zhang, F. J.; Li, X. H. Poly-l-lysine assisted synthesis of core-shell nanoparticles and conjugation with triphenylphosphonium to target mitochondria. *J. Mater. Chem. B* **2013**, *1* (38), 5143–5152.

(33) He, H.; Liu, B.; Wen, S.; Liao, J.; Lin, G.; Zhou, J.; Jin, D. Quantitative Lateral Flow Strip Sensor Using Highly Doped

Upconversion Nanoparticles. *Anal. Chem.* **2018**, *90* (21), 12356–12360.

(34) Liu, P. Y.; Chin, L. K.; Ser, W.; Chen, H. F.; Hsieh, C. M.; Lee, C. H.; Sung, K. B.; Ayi, T. C.; Yap, P. H.; Liedberg, B.; Wang, K.; Bourouina, T.; Leprince-Wang, Y. Cell refractive index for cell biology and disease diagnosis: past, present and future. *Lab Chip* **2016**, *16* (4), 634–44.

(35) Takei, Y.; Arai, S.; Murata, A.; Takabayashi, M.; Oyama, K.; Ishiwata, S. i.; Takeoka, S.; Suzuki, M. A Nanoparticle-Based Ratiometric and Self-Calibrated Fluorescent Thermometer for Single Living Cells. *ACS Nano* **2014**, *8* (1), 198–206.

(36) Yang, J.-M.; Yang, H.; Lin, L. Quantum Dot Nano Thermometers Reveal Heterogeneous Local Thermogenesis in Living Cells. *ACS Nano* **2011**, *5* (6), 5067–5071.

(37) Cutro, A. C.; Montich, G. G.; Roveri, O. A. Effect of carbonylcyanide-4-(trifluoromethoxy)phenylhydrazone (FCCP) on the interaction of 1-anilino-8-naphthalene sulfonate (ANS) with phosphatidylcholine liposomes. *J. Bioenerg. Biomembr.* **2014**, *46* (2), 119–25.

(38) Wang, X.-H.; Peng, H.-S.; Yang, L.; You, F.-T.; Teng, F.; Hou, L.-L.; Wolfbeis, O. S. Targetable Phosphorescent Oxygen Nanosensors for the Assessment of Tumor Mitochondrial Dysfunction By Monitoring the Respiratory Activity. *Angew. Chem.* **2014**, *126* (46), 12679–12683.

(39) Chretien, D.; Benit, P.; Ha, H. H.; Keipert, S.; El-Khoury, R.; Chang, Y. T.; Jastroch, M.; Jacobs, H. T.; Rustin, P.; Rak, M. Mitochondria are physiologically maintained at close to 50 degrees C. *PLoS Biol.* **2018**, *16* (1), No. e2003992.

(40) Hu, S.; Liu, B. J.; Feng, J. M.; Zong, C.; Lin, K. Q.; Wang, X.; Wu, D. Y.; Ren, B. Quantifying Surface Temperature of Thermoplasmonic Nanostructures. *J. Am. Chem. Soc.* **2018**, *140* (42), 13680–13686.

(41) Nakano, M.; Arai, Y.; Kotera, I.; Okabe, K.; Kamei, Y.; Nagai, T. Genetically encoded ratiometric fluorescent thermometer with wide range and rapid response. *PLoS One* **2017**, *12* (2), No. e0172344.

(42) Chen, R.; Ta, V. D.; Xiao, F.; Zhang, Q.; Sun, H. Multicolor hybrid upconversion nanoparticles and their improved performance as luminescence temperature sensors due to energy transfer. *Small* **2013**, *9* (7), 1052–7.

(43) Yang, X.; Yang, Z.; Wu, Z.; He, Y.; Shan, C.; Chai, P.; Ma, C.; Tian, M.; Teng, J.; Jin, D.; Yan, W.; Das, P.; Qu, J.; Xi, P. Mitochondrial dynamics quantitatively revealed by STED nanoscopy with an enhanced squaraine variant probe. *Nat. Commun.* **2020**, *11* (1), 3699.

(44) Su, Q. P.; Zhao, Z. W.; Meng, L.; Ding, M.; Zhang, W.; Li, Y.; Liu, M.; Li, R.; Gao, Y. Q.; Xie, X. S.; Sun, Y. Superresolution imaging reveals spatiotemporal propagation of human replication foci mediated by CTCF-organized chromatin structures. *Proc. Natl. Acad. Sci. U. S. A.* **2020**, *117* (26), 15036–15046.

(45) Chen, Y.; Su, Q. P.; Sun, Y.; Yu, L. Visualizing Autophagic Lysosome Reformation in Cells Using In Vitro Reconstitution Systems. *Current Protocols in Cell Biology* **2018**, *78* (1), 11.24.1–11.24.15.

(46) Xu, M.; Zou, X.; Su, Q.; Yuan, W.; Cao, C.; Wang, Q.; Zhu, X.; Feng, W.; Li, F. Ratiometric nanothermometer in vivo based on triplet sensitized upconversion. *Nat. Commun.* **2018**, *9* (1), 2698.

(47) Chung, D. J.; Healy, T. M.; McKenzie, J. L.; Chicco, A. J.; Sparagna, G. C.; Schulte, P. M. Mitochondria, Temperature, and the Pace of Life. *Integr. Comp. Biol.* **2018**, *58* (3), 578–590.